


# A Method for Interval Prediction of Satellite Battery State of Health Based on Sample Entropy

MENGDA CAO<sup>1</sup>, TAO ZHANG<sup>1</sup>, BIN YU<sup>2</sup>, AND YAJIE LIU<sup>1</sup> 

<sup>1</sup>College of System Engineering, National University of Defense Technology, Changsha 410073, China

<sup>2</sup>China Aerospace Science and Technology Corporation, Beijing 100048, China

Corresponding author: Yajie Liu (liuyajie@nudt.edu.cn)

This work was supported in part by the National Natural Science Foundation of China under Grant 71571187, and in part by the Excellent Youth Foundation of Hunan Scientific Committee under Grant 2017JJ1001.

**ABSTRACT** Satellites need batteries to provide energy when operating in shadow regions, and lithium-ion batteries have become the batteries of choice for most satellites due to their high energy density, low self-discharge rate, and long cycle life. When a satellite battery is working in outer space, its capacity will gradually decrease as the number of cycles increases, and a certain degree of capacity recovery will occur. Due to the excellent mapping relationship between the discharge cutoff voltage and the capacity degradation of lithium-ion batteries and the fact that the sample entropy (SampEn) can sensitively capture local fluctuations, such as the recovery effect during lithium-ion battery capacity degradation, a method for interval prediction of the satellite battery state of health (SOH) based on SampEn was proposed. This method adopts a neural network model based on lower upper bound estimation (LUBE). The method uses the discharge cutoff voltage and the discharge voltage SampEn as the inputs and the battery SOH as the output for the neural network model. To improve the prediction interval coverage and reduce the prediction interval width, especially considering that the lower bound of the interval prediction often determines whether the satellite battery output power reaches the warning threshold, a modified comprehensive indicator function, the coverage width-based criterion (CWC), was constructed. Additionally, based on the nondifferentiability of this indicator function, a simulated annealing algorithm was used to optimize the neural network; at the same time, the optimal values of the interval coverage and interval width were taken into account, resulting in the lower bound of the prediction interval being closer to the actual value. Finally, test data from a NASA #18 battery were used to validate, analyze and verify the interval prediction algorithm proposed in this paper. The results were compared with those obtained from a support vector machine (SVM)-based interval prediction method.

**INDEX TERMS** Battery state of health (SOH), sample entropy (SampEn), lower upper bound estimation (LUBE), neural network, simulated annealing.

## I. INTRODUCTION

In recent years, an increasing number of satellites have been launched into space to provide data for various tasks, including weather forecasting, resource observation, and geological surveys. The power system is key for the normal operation of satellites in space, and its availability, reliability, and sustainability are critical. Power systems usually combine a variety of energy storage technologies, such as batteries and solar cells, to provide a safe and reliable power supply for satellites [1], [2]. Once the power system is damaged, many parts

of the satellite will lose function and cannot continue to perform tasks [3]. The battery is the only source of energy when the satellite is operating in a shadow region. Once abnormal battery conditions occur, the satellite will not be able to work in the shadow region. Therefore, the satellite battery life has become the largest ‘ceiling’ constraining the development of spacecraft. The performance of the satellite battery will gradually degrade as the working hours increase. This degradation will result in an insufficient amount of energy being supplied to the satellite in the shadow region. The related loads will then not work properly, thus affecting the overall performance of the satellite and resulting in expensive maintenance and serious damage. Therefore, constructing an effective model

The associate editor coordinating the review of this manuscript and approving it for publication was Jiajie Fan.

of battery performance degradation based on the extraction of characteristic indicators that measure the degradation of the spacecraft battery performance is important in actual practice.

Numerous types of satellite batteries have been developed. Lithium-ion batteries have become the third-generation satellite energy storage batteries, replacing nickel-hydrogen and nickel-cadmium batteries due to their high energy density, low self-discharge rate, long cycle life, and wide operating temperature range; these batteries have been used in various engineering applications [4], [5]. For example, lithium-ion batteries were used as the energy storage power source in the National Aeronautics and Space Administration (NASA)'s Spirit and Opportunity Mars exploration rovers and the Phoenix Mars lander, the European Space Agency (ESA)'s Mars Express and ROSETTA platform, and the Japanese Hayabusa spacecraft [6]. Under these circumstances, the performance degradation and the health assessment of satellite lithium-ion batteries have become a research topic of interest. Many studies have focused on monitoring the state of lithium-ion batteries, assessing their health, etc., and some classic parameters of the battery state have been proposed, such as the state of charge (SOC) and state of health (SOH) [7], [9].

The SOH characterizes the capacity of a battery to store electrical energy and provide energy relative to a new battery and is an indicator that quantitatively describes the state of battery performance. As charge and discharge occur, the battery SOH trends downward [10], [11]. At present, SOH assessment for batteries is mainly based on models and data-driven methods. The model-based methods involve modeling mechanisms on the basis of the physical and chemical characteristics of the battery, simulating the dynamic characteristics and the degradation process of the battery, and applying a model parameter identification algorithm to assess the SOH [12], [13]. The model-based methods include the electrochemical model, the equivalent circuit model, and the impedance spectrum model. Although the physical meaning of model-based SOH assessment is clear, the models are generally complex, their assessment accuracy is generally not high, and the methods are not universal, exhibiting poor real-time performance. With the rapid development of machine learning and artificial intelligence, data-driven methods have gradually entered the research field and are now widely used in battery SOH assessment [14]. Compared with the experiment- and mechanism-based modeling methods, the data-driven methods ignore the electrochemical principles to some extent and rely on various mapping and regression tools to develop the degradation model. Wu *et al.* [15] proposed using the importance of sampling (IS) as the input for a feedforward neural network, simulating the relationship between the remaining useful life (RUL) and the charging curve. Ng *et al.* [16] selected the naïve Bayes method to predict the RUL of a lithium-ion battery and compared and verified the results with those obtained using a support vector machine (SVM)-based method. Zhang *et al.* [17] proposed a jump diffusion process with a nonhomogeneous

compound Poisson process to model the degradation process with randomly occurring jumps. In addition, many researchers have proposed mathematical functions to estimate battery SOH. Chen *et al.* [18] proposed an adaptive bathtub-shaped failure-rate function (ABF) and used the artificial fish-swarm algorithm to optimize the ABF function and simulate the battery cycle capacity curve. Wang *et al.* [19] constructed a conditional three-parameter lithium-ion battery RUL model using an exponential function and an SVM algorithm.

Related studies have shown that during the degradation process caused by an increase in the number of cycles, lithium-ion batteries often exhibit local fluctuations such as capacity recovery effects. This phenomenon generally occurs after the battery has been working for several cycles. If the battery is left to rest for a period of time, then its capacity will recover to some extent. This phenomenon occurs because lithium ions gradually form two types of compounds during charge and discharge. One type includes stable compounds, which are difficult to decompose, resulting in permanent degradation of the capacity of lithium-ion batteries. The other type includes unstable compounds. When the battery is left in a resting state, the unstable compounds will decompose, thus regenerating lithium ions, which will restore the battery capacity to some extent [20]–[22]. In the aforementioned methods, the battery capacity in the aging cycle is directly analyzed. Thus, taking the self-recovery phenomena into consideration in the SOH prognostics of a lithium-ion battery is meaningful.

Thus far, this issue has not been solved well, and only a few researchers have focused on it [23]. Some researchers have presented that capacity recovery has a certain regularity over time. Eddahech *et al.* [24] constructed a battery power aging experiment under two temperatures (45°C and 55°C) with different combinations of power cycling and proved that the battery capacity recovery phenomenon is dependent on the Stop-SOC. Liu *et al.* [25] used a combination of the covariance function and the averaging function to improve the multistep prediction of Gaussian process regression (GPR), thereby predicting SOH recovery and degradation. He *et al.* [26] used the wavelet method to analyze global degradation and local recovery and proposed a multiscale GPR modeling method to tackle the accurate SOH estimation problem. However, the capacity recovery phenomenon is related to the rest time, and the rest time is determined by the actual working conditions of the battery. Therefore, accurately predicting the recovery phenomenon without considering the rest time is difficult. Some researchers considered the capacity recovery as an uncertainty. Zhang *et al.* [23] proposed a multiphase stochastic degradation model with random jumps based on the Wiener process, where the multiphase model and random jumps at the changing point are used to describe the variations in the degradation rate and state caused by regeneration phenomena. Olivares *et al.* [27] estimated the SOH and predicted the RUL while simultaneously detecting and isolating the effect of self-recovery phenomena

within the life-cycle model. Tao and Lu [28] extracted some features affecting the battery capacity recovery and used a random forest (RF) to model and cognize the capacity degradation process. However, researchers still hope to extract a reliable and effective degradation indicator and construct a mapping relation between indicators and the actual capacity when constructing a SOH prognostic model. The trend of battery capacity degradation can thereby be effectively fitted, and the local fluctuations that reflect the actual battery SOH can be captured.

In this regard, researchers have introduced a characteristic parameter, the sample entropy (SampEn), for local fluctuations in the process of lithium-ion capacity degradation. SampEn, as a useful tool for exploring signal complexity and predictability [29], can be introduced as a characteristic parameter for diagnosing battery capacity degradation due to its relatively sensitive response to changes in complexity and fluctuations. Sun *et al.* [30] proposed extracting SampEn from the discharge voltage of lead-acid batteries in series as an indicator of aging. Hu *et al.* [31] used the battery voltage SampEn under the hybrid pulse power curve as the input and established a battery degradation model by least-squares optimization. Hu *et al.* [32] extracted the SampEn of a short-voltage sequence as the degradation characteristic and used the sparse Bayesian predictive modeling (SBPM) method to capture the mapping relation between battery capacity degradation and SampEn. Li *et al.* [33] combined the particle filter (PF) and SampEn characteristics of the discharge voltage to predict the remaining capacity of lithium-ion batteries. Li *et al.* [34] extracted SampEn from the surface temperature in the lithium-ion battery charging process and combined it with the PF to develop an intelligent estimation method for capacity degradation. In addition, some authors have directly selected the voltage and current changes during battery charging and discharging to extract degradation characteristics. For example, Wang *et al.* [35] used the current curve changes during constant battery current-constant voltage charging to characterize the battery SOH.

The aforementioned predictions of the remaining battery capacity are mainly based on point predictions, and most of the research has focused on how to improve the accuracy of the point prediction method and how to effectively capture the local fluctuations in the capacity prediction. However, due to the uncertainties in the variables and the environment, the prediction based on the point prediction method always exhibits an error, which is difficult to eliminate. When the prediction error is large, it often affects the ground system personnel's judgment and the operation of the satellite on-orbit state. In fact, the ground operators' prediction of the battery SOH often requires a reasonable interval range; that is, the interval should contain both the actual capacity and the possible range of fluctuations so that the operators can detect abnormal fluctuations of the battery as early as possible and adjust the working state of the satellite in time.

As stated above, researchers have proposed two types of approaches to construct prediction intervals for the battery SOH. The first type includes theoretical approaches. For these approaches, the theoretical interval is calculated based on the assumption that forecast errors follow a determined distribution with zero mean, usually the normal distribution or Laplace distribution [36]. For instance, Wang *et al.* [37] filtered the IC curve to extract the peak value and position as health factors and established a SOH estimation model based on GPR. Li *et al.* [38] developed a multistep-ahead prediction model based on the mean entropy and a relevance vector machine (RVM). Both methods construct 95% confidence bounds of the prediction results based on a Gaussian distribution. Nevertheless, as the data in actual practice always involve complex processes, ensuring that the Gaussian assumption can be fulfilled is difficult. The theoretical prediction interval may behave poorly if the aforementioned assumption is not valid. As an alternative, the second type of approaches with no need for consideration of the forecast error distribution has been proposed. The neural network approach is typical of such approaches. In the field of lithium-ion batteries, some studies on constructing prediction intervals for capacity estimation based on the previously mentioned error distribution have been performed. However, directly constructing an interval for predicting the battery capacity is little studied.

Based on the lower upper bound estimation (LUBE) neural network model, we propose a SOH interval prediction model. This method selects the discharge cutoff voltage in the discharge cycle of the lithium-ion battery and the SampEn extracted from the output voltage as the inputs and the lithium-ion battery SOH as the output. The advantages of our interval prediction method for battery SOH mainly include three aspects: (1) The degradation characteristics of SampEn not only can provide degradation information of the battery but also are sensitive to the local fluctuations within the life cycle. Thus, this model can accurately estimate the SOH of batteries and capture the self-recovery phenomenon. (2) Compared to the theoretical interval prediction method, the method proposed in this paper can provide reliable and effective prediction intervals without the need for an error distribution. (3) Because the lower bound of the interval prediction often determines the minimum power supply capacity of the battery, a new comprehensive indicator, the coverage width-based criterion (new CWC) is constructed to allow the lower bound to be close to the actual value while improving the interval coverage and reducing the interval width. Finally, based on the lithium-ion battery aging dataset from the NASA Ames Prognostics Center of Excellence (PCoE), the validity of the proposed SOH interval prediction method is verified. This method is compared with the existing SVM prediction method, and the feasibility and advantages of the proposed model method are verified.

The remainder of the paper is organized as follows. Section 2 describes the extraction process of the degradation characteristics and the modeling principle of the LUBE

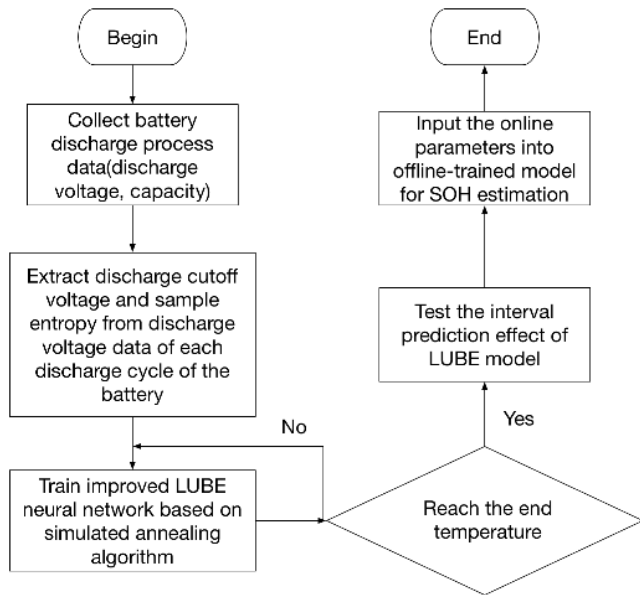


FIGURE 1. Flowchart of the satellite battery interval prediction method.

neural network. Section 3 presents the experimental data and result analysis. A comparison experiment with the SVM method is reported in Section 4. Finally, Section 5 concludes the paper and discusses future work.

## II. INTERVAL PREDICTION METHOD FOR THE SATELLITE BATTERY SOH

The flowchart of the satellite battery interval prediction method proposed in this paper is shown in Fig. 1. First, the voltage and capacity data during the discharge process of the battery were collected. Then, the SOH was estimated using the capacity approach. At present, SOH estimation of lithium-ion batteries still has many problems, which are mainly reflected in two aspects: (1) Simple and effective methods for analyzing the battery aging process are lacking. (2) The battery SOH online estimation method is not mature, and the real-time performance is poor. The only reliable method to calculate the SOH is discharging the battery completely with a load. Because the PCoE battery cycle experiment involves complete discharge, the SOH is normally defined as the ratio between the actual battery capacity and nominal battery capacity, represented as [39]

$$SOH = \frac{\text{nominal capacity at present time}}{\text{nominal capacity at initial time}} \quad (1)$$

Moreover, SampEn was constructed based on the discharge voltage data sequence; in addition, the discharge cutoff voltage was extracted from the discharge voltage data sequence. Second, based on the discharge cutoff voltage, SampEn, and the battery capacity data sequence, a neural network model based on LUBE was constructed and trained. In this process, a simulated annealing algorithm was used to optimize the model parameters. Finally, based on the experimental data on related lithium-ion batteries disclosed by NASA, the validity

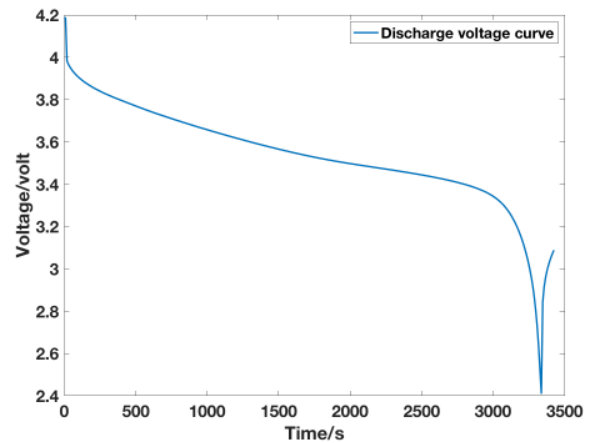


FIGURE 2. Discharge voltage curve of a lithium-ion battery.

of the prediction method proposed in this paper was verified. The training model process is offline. We can obtain the SOH estimation by inputting the online parameters into the offline-trained model. The following sections describe the extraction of the degradation characteristics of the lithium-ion battery and the construction and optimization of the LUBE neural network.

### A. EXTRACTION OF DEGRADATION CHARACTERISTICS

#### 1) DISCHARGE CUTOFF VOLTAGE

When the satellite enters a shadow region, the battery provides the power for satellite operation. At this time, the battery starts to discharge, and the discharge voltage gradually decreases as the discharge process proceeds. The lowest voltage corresponding to the end of the discharge is the discharge cutoff voltage, as shown in Fig. 2.

Due to the degradation of the satellite battery performance, after the battery is fully charged, the discharge cutoff voltage reached after the same amount of power is discharged while the discharge current is kept constant becomes lower over time. Therefore, the discharge cutoff voltage was used as one of the characteristic quantities for analyzing battery performance in this study.

However, when only the discharge cutoff voltage is used as the input to the neural network to construct the degradation model, although the overall degradation trend is well fitted, the model is not sensitive to local fluctuations, such as the capacity recovery effect during the degradation of the lithium-ion battery. Therefore, based on the selection of the discharge cutoff voltage as a characteristic quantity, in this study, we further selected another parameter, SampEn, to enhance the sensitivity of the neural network model to the capacity recovery effect. The meaning of SampEn is described below.

#### 2) SAMPLE ENTROPY (SampEn)

Pincus [40] proposed the approximate entropy (ApEn) when measuring the complexity of a time series, and SampEn was obtained from a modification of ApEn. ApEn is used to solve

the noise problem in time series and is a nonlinear dynamic parameter that quantifies the regularity and unpredictability of the fluctuations of a time series. SampEn has the same physical meaning as the approximate entropy and measures the complexity of the time series by measuring the probability of generating new patterns in the signal. The greater the probability of a new pattern is, the greater the complexity of the sequence [41]. Compared with ApEn, SampEn exhibits two advantages [42]:

(1) The calculation of SampEn does not depend on the data length.

(2) SampEn is more consistent.

In general, the lower the SampEn value is, the higher the sequence self-similarity; the larger the SampEn value is, the more complex the sample sequence. The internal complexity of a lithium-ion battery varies with the degradation of the battery; thus, the SampEn of the voltage sequence could be an effective signature correlated to battery health. At present, SampEn has been applied in the analysis of wind-power generation, heat-exchange performance, heart-rate variability, and time series of diagnostic cases [43]–[45].

(1) A sequence of vectors of length  $m$  is selected according to the sequence number of the time series, where  $\{x(n)\} = x(1), x(2), \dots, x(N)$ . This set of vectors represents  $m$  consecutive values starting from the  $i$ th point in the  $N$  number of data points.

(2) The distance between the vector  $X_m(i)$  and the vector  $X_m(j)$  is defined as the absolute value of the maximum difference between the elements corresponding to the two sets of vectors:

$$d[X_m(i), X_m(j)] = \max_{k=0, \dots, m-1} (|x(i+k) - x(j+k)|) \quad (2)$$

(3) For a given  $X_m(i)$ , the number of  $j(1 \leq j \leq N-m, j \neq i)$  with a distance between  $X_m(i)$  and  $X_m(j)$  less than or equal to  $r$  is calculated and denoted  $B_i$ :

$$B_i^m(r) = \frac{1}{N-m-1} B_i \quad (3)$$

(4)  $B^m(r)$  is defined as

$$B^{(m)}(r) = \frac{1}{N-m} \sum_{i=1}^{N-m} B_i^m(r) \quad (4)$$

(5) The dimension is increased to  $m+1$ , and the number of  $j(1 \leq j \leq N-m, j \neq i)$  with a distance between  $X_{m+1}(i)$  and  $X_{m+1}(j)$  less than or equal to  $r$  is calculated and denoted  $A_i^m$ .  $A_i^m$  is defined as

$$A_i^m(r) = \frac{1}{N-m-1} A_i \quad (5)$$

(6) We define  $A^m(r)$  as

$$A^{(m)}(r) = \frac{1}{N-m} \sum_{i=1}^{N-m} A_i^m(r) \quad (6)$$

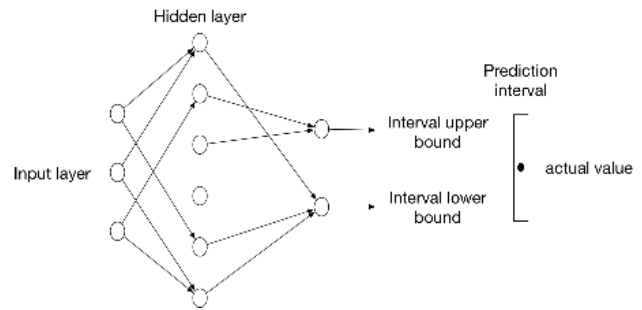


FIGURE 3. Architecture of the LUBE neural network.

Thus,  $B^m(r)$  is defined as the probability that two sequences will match for  $m$  points with a tolerance of  $r$ , while  $A^m(r)$  is the probability that two sequences will match for  $m+1$  points. SampEn is defined as follows:

$$\text{SampEn}(m, r) = \lim_{N \rightarrow \infty} -\ln \left[ \frac{A^m(r)}{B^m(r)} \right] \quad (7)$$

Since SampEn exhibits good consistency, the values of  $m$  and  $r$  share some characteristics with respect to their influences on SampEn. Generally,  $m$  is 1 or 2, and  $r$  is 0.1. When  $N$  is a finite number, Eq. (7) can be expressed as

$$\text{SampEn}(m, r, N) = -\ln \left[ \frac{A^m(r)}{B^m(r)} \right] \quad (8)$$

## B. CONSTRUCTION AND OPTIMIZATION OF THE LUBE NEURAL NETWORK

The structure of the LUBE neural network, as a type of interval prediction neural network, is shown in Fig. 3. The final output is the upper and lower bounds of an estimated value. Specifically, the prediction interval is composed of a lower limit  $L_i$  and an upper limit  $U_i$ ; the predicted target value  $y_i$  exists in the prediction interval with a certain probability, and this probability is called the confidence level. The assessment of the quality of a prediction interval is usually based on two indicators: the prediction interval coverage probability (PICP) and the normalized mean prediction interval width (NMPIW). The PICP and the NMPIW have been widely used as assessment indicators for prediction intervals in related studies [46].

For a constructed prediction interval, assuming that the actual value is within the constructed predicted interval with a probability of  $1 - \alpha$ , we generally expect a prediction interval with greater coverage. Therefore, the PICP is an important factor in assessing the prediction interval. The interval coverage is measured by calculating how many actual values are within the prediction interval. The equation is

$$\text{PICP} = \frac{1}{N} \sum_{i=1}^N c_i \quad (9)$$

where  $N$  is the number of samples in the test set. The equation to calculate  $c_i$  is as follows. When the actual value  $t_i$  falls

between the upper and lower bounds of the constructed prediction interval,  $c_i$  is 1; otherwise,  $c_i$  is 0:

$$c_i = \begin{cases} 1, & \text{if } t_i \in [L_i, U_i] \\ 0, & \text{if } t_i \notin [L_i, U_i] \end{cases} \quad (10)$$

Here  $U_i$  is the upper bound of the prediction interval, and  $L_i$  is the lower bound of the prediction interval. Ideally, the PICP should be very close to or greater than the confidence level of the prediction interval. If the PICP is 0, then no actual value falls within the interval. If the PICP is 1, then all of the actual values fall within the interval. The larger the PICP value is, the better the interval quality. If the upper and lower limits of the interval are the minimum and maximum of all predicted targets, respectively, then the corresponding PICP will be a perfect 100%. However, an excessively wide prediction interval does not provide any meaningful information to decision makers. Therefore, while considering the interval coverage, the width of the prediction interval should also be considered. The MPIW is defined as follows:

$$MPIW = \frac{1}{N} \sum_{i=1}^N (U_i - L_i) \quad (11)$$

In practical applications, the NMPIW is generally used to measure the interval width, which is defined as

$$NMPIW = \frac{MPIW}{R} \quad (12)$$

where  $R$  is the value range of the targets to be tested; the smaller the NMPIW value is, the better the interval quality.

The range for both the PICP and NMPIW is  $[0, 1]$ . Increasing the interval coverage usually means increasing the interval width, while narrowing the interval width tends to reduce the interval coverage. Therefore, the two targets have mutually exclusive characteristics. In view of the mutually exclusive characteristics of these two objectives, in this study, we used the traditional integrated indicator CWC to combine these two indicators. The specific definitions are as follows:

$$CWC = NMPIW \cdot \left(1 + \gamma(PICP)e^{-\eta(PICP-\mu)}\right) \quad (13)$$

where  $\gamma(PICP)$  is defined as

$$\gamma = \begin{cases} 1, & \text{if } PICP < \mu \\ 0, & \text{if } PICP \geq \mu \end{cases} \quad (14)$$

However, in the satellite battery SOH prediction process, the SOH is the ratio of the actual capacity to the standard capacity and characterizes the power supply capability of the battery. The lower bound of the prediction interval determines the minimum power supply capacity of the battery. Once the lower bound of the prediction interval is lower than the warning threshold, the ground operators usually need to adjust the satellite working state in time. Thus, the lower bound of the prediction interval is correlated with the battery SOH. Related literature about biased interval prediction has been presented. Marín added an error quantity function for mid-interval consideration-based wind-power generation and

load-forecasting systems [47]. The error quantity is defined by the following equation:

$$\|e\| = \sqrt{\sum_{j=1}^n \left| t_j - \frac{\bar{y}_j + \underline{y}_j}{2} \right|^2} \quad (15)$$

where  $t_j$  is the value of the  $j^{th}$  sample.  $\bar{y}_j$  and  $\underline{y}_j$  are the upper and lower bounds of the prediction interval. Therefore, based on the actual demand of the satellite battery SOH prediction and abovementioned error quantity function, the interval width and the interval coverage should be guaranteed. Additionally, if the difference between the lower bound of the interval prediction and the actual value is too large, then the ground operator may adjust the battery too early. We propose a new integrated indicator CWC, represented as

$$CWC = \beta_1 \cdot NMPIW + \beta_2 \cdot e^2 + \gamma \cdot \exp[-\eta(PICP - \mu)] \quad (16)$$

where  $\beta_1$  and  $\beta_2$  are the weight coefficients used to normalize the NMPIW and  $e$ ; the parameter  $e$  represents the number of interval prediction deviations, as described in the following equation:

$$e = \sum_{i=1}^N |(SOH_{true} - lower_i)| \quad (17)$$

where  $SOH_{true}$  is the actual capacity of the battery at the  $i^{th}$  cycle and  $Lower_i$  is the lower bound of the interval prediction for this cycle.

Based on the above-modified integrated indicator, the LUBE is modified. That is, the interval quality is included through two basic assessment indicators, the PICP and NMPIW. At the same time, the number of interval deviations is added such that the lower bound of the interval prediction is closer to the actual value. The modified LUBE adopts the three-indicator integrated indicator CWC as the loss function. Since the function is nondifferentiable, the heuristic simulated annealing algorithm is used to optimize the network structure.

The flowchart of the basic algorithm is shown in Fig. 4. The specific steps and meanings are as follows:

(1) Data preparation: The original data are divided into two parts, i.e., the training set and the test set. The training set is used for model training, and the test set is used to test the algorithm performance and carry out the data normalization.

(2) Parameter initialization: The parameter of the neural network  $w_{opt}$  and the parameters of the simulated annealing algorithm, such as the initial temperature and initial indicator value  $CWC_{opt}$ , are initialized.

(3) A temperature update is performed until the temperature reaches the threshold.

(4) A new neural network parameter  $w_{opt}$  is generated by perturbation, and the neural network parameters are used to construct a prediction interval and calculate the new indicator value  $CWC_{opt}$ . If the new indicator value is better than the

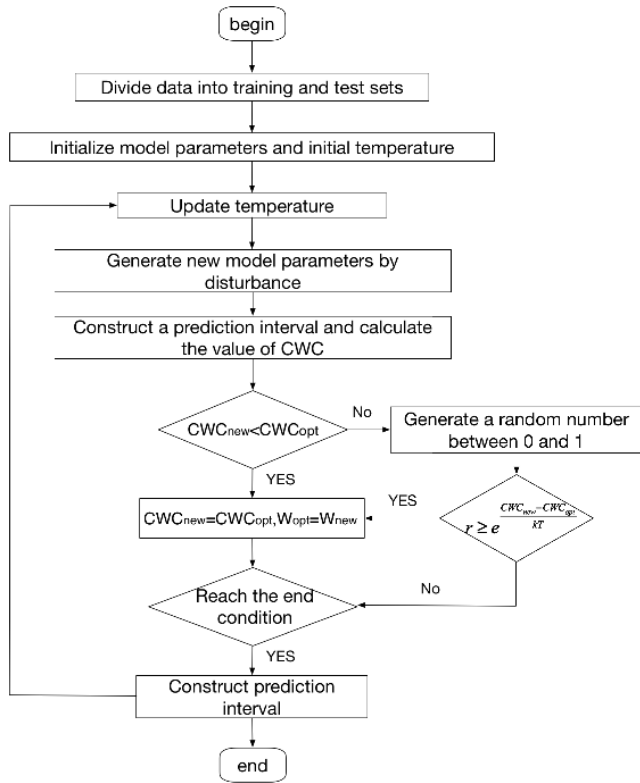


FIGURE 4. Flowchart of the LUBE neural network optimization based on the simulated annealing algorithm.

old one, i.e.,  $CWC_{new} < CWC_{opt}$ , then  $CWC_{opt} = CWC_{new}$  and  $w_{opt} = w_{new}$ . Otherwise, a random number is generated. If  $r \geq e^{-\frac{(CWC_{new} - CWC_{opt})}{\kappa T}}$  is satisfied, then the new solution is still accepted; that is, the new solution is accepted with a certain probability.

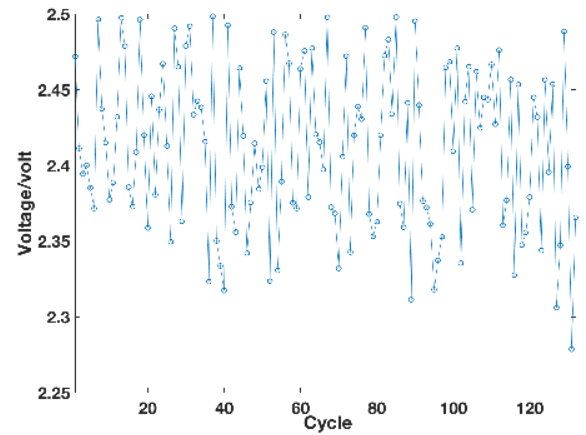
(5) If the temperature reaches the threshold, training is stopped, and step (6) is carried out; otherwise, the procedure is repeated from step (3).

(6) The resulting neural network is used to perform interval prediction on the test set and to assess the performance of the model according to the assessment indicator.

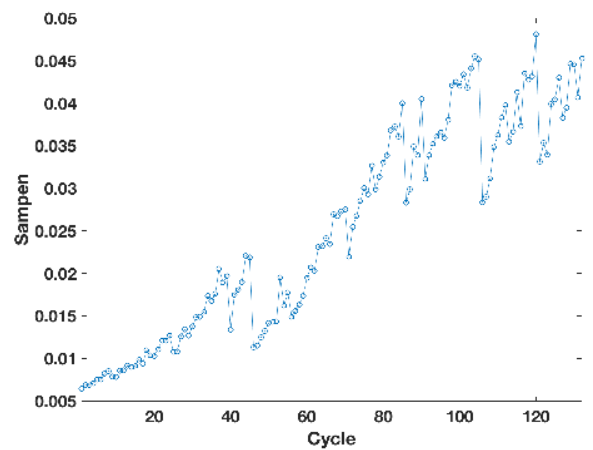
### III. EXPERIMENTAL VALIDATION

#### 1) EXPERIMENTAL DATA

The lithium-ion battery data used in this paper were derived from the lithium-ion battery aging dataset published by the NASA Ames PCoE for experimental validation. The lithium-ion battery data were collected at the Idaho National Laboratory using a commercially available 18650 lithium-ion battery with a rated capacity of 2 Ah. In the experiment, the battery was charged with a constant current of 1.5 A under three conditions (charge, discharge, and impedance) at 24°C. After the voltage reached 4.2 V, the battery discharged at a constant current of 2 A until the voltage decreased to the cutoff voltage. During each cycle, the battery had the same depth of discharge. During the continuous charge and discharge cycles, the actual capacity of the battery was



(a) Discharge cutoff voltage changes with cycle



(b) Sample entropy (SampEn) changes with cycle

FIGURE 5. Discharge cutoff voltage and SampEn curves for the #18 battery.

collected, and impedance measurements were carried out by electrochemical impedance spectroscopy (EIS) at frequencies from 0.1 kHz to 5 kHz.

Since lithium-ion batteries consume chemical components such as electrolytes, positive and negative electrodes, and separators during energy conversion, irreversible degradation occurs inside the battery. The actual capacity of a lithium-ion battery will gradually decrease as the number of charge and discharge cycles increases. In Fig. 5, the discharge cutoff voltage and the SampEn of the discharge voltage for each discharge cycle extracted from the PCoE dataset for the #18 battery are shown. When SampEn was extracted,  $m$  and  $r$  were set to 1 and 0.1, respectively. As shown in the figure, SampEn increased as the number of cycles increased, and the discharge cutoff voltage gradually decreased as the number of cycles increased. In Fig. 6, the capacity degradation curve of the #18 battery after normalization, i.e., Min-Max scaling, is shown. The data show that as the number of cycles increased, the capacity gradually decreased until it reached the failure threshold. The charge and discharge cycle experiment from the PCoE dataset will be ended when the

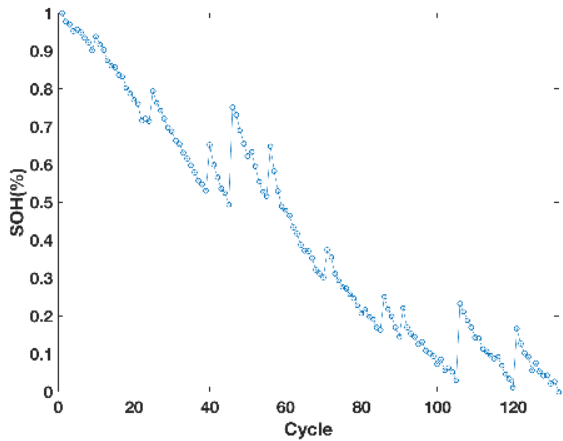


FIGURE 6. Capacity degradation curve of the #18 battery.

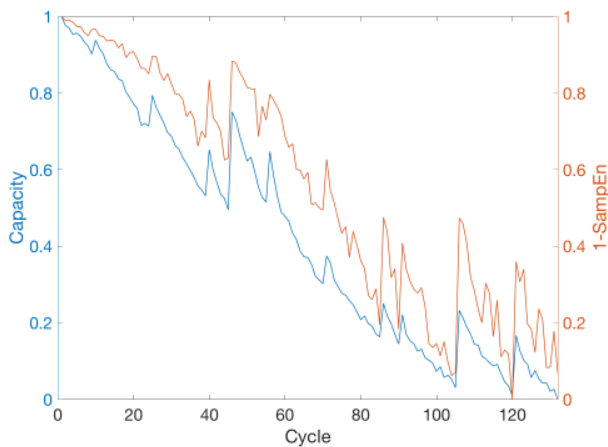


FIGURE 7. Relation between SampEn and battery capacity.

capacity of the lithium-ion battery reached a 30% fade (from 2 Ah to 1.4 Ah).

2) SampEn AND CAPACITY DEGRADATION

As the lithium-ion battery was continuously charged and discharged, its capacity rapidly decreased as the number of cycles increased. The NASA battery degradation experiment designer set several rests after a period of continuous charge and discharge cycles to enable researchers to better investigate the capacity recovery effects. The SampEn and the actual capacity were normalized, and the measured changes in the battery capacity and SampEn were collected as the number of cycles increased. In Fig. 7, the curves of the changes in the two characteristic parameters of the #18 battery with increasing number of cycles are shown. The data in the figure show an interesting phenomenon. That is, in the 46<sup>th</sup> cycle and the 105<sup>th</sup> cycle of the #18 battery, the lithium-ion battery exhibited some capacity recovery, while the SampEn decreased with this increase in capacity, showing that SampEn can sensitively capture the capacity recovery effect of a lithium-ion battery.

The sensitive capture of the capacity recovery effect of lithium-ion batteries by SampEn is mainly possible because

TABLE 1. LUBE neural network and simulated annealing initial parameter settings.

Parameter	$\mu$	$\gamma$	$\beta_1$	$\beta_2$	$Iter$	$T_{begin}$	$T_{end}$	$Bolt$
Value	0.9	50	0.3	0.01	0.9	10000	0.001	0.7

SampEn measures the complexity of a time series by measuring the probability of generating a new pattern in the signal. In essence, SampEn expresses the degree of disorder (complexity) of the time series. The capacity recovery effect is caused by unstable compounds and their decomposition during the charging and discharging process of lithium-ion batteries. In the process of unstable compounds being generated by lithium ions, the degree of disorder of the metal compounds is higher than that of the metal ions [48], [49]; thus, this process is an entropy-increasing process. However, after the decomposition of the unstable compounds, the whole system tends to be stable, and the degree of disorder is reduced, which is an entropy-decreasing process. Therefore, when the capacity recovery effect occurs, the degree of disorder of the system temporarily increases due to the formation of unstable compounds, the actual capacity of the battery briefly decreases, and SampEn briefly increases. When the unstable compounds decompose, the degree of disorder of the system decreases, the actual capacity increases, and SampEn accordingly decreases.

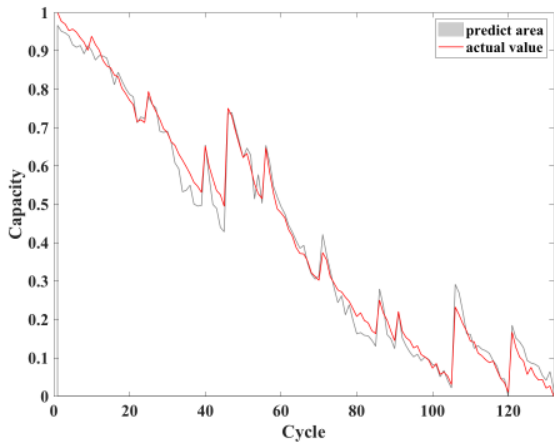
A. PERFORMANCE OF THE INTERVAL PREDICTION ALGORITHM

To verify the effectiveness of the modified LUBE neural network model proposed in this paper, the discharge cutoff voltage and the SampEn of the NASA #18 battery were selected as the inputs of the prediction model, and the SOH was selected as the output of the prediction model. In the training process for the neural network model, the neural network parameters were optimized by the simulated annealing algorithm. In this dataset, the first 90% of the data is selected as the training set, and the remaining 10% is utilized as the verification set. The LUBE neural network and simulated annealing parameter settings were as shown in Table 1.

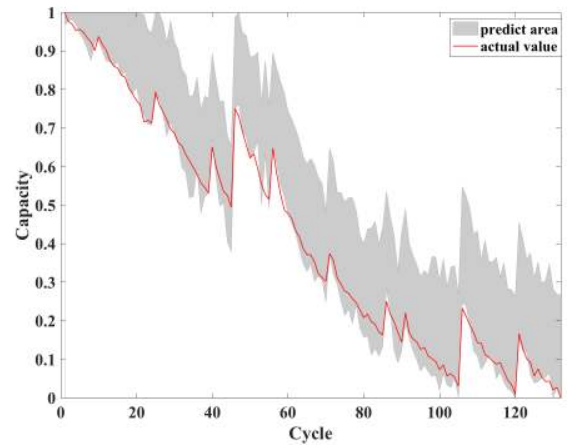
Here,  $\mu$  and  $\gamma$  are hyperparameters that adjust the quality of the prediction interval, and  $\beta_1$  and  $\beta_2$  are the weighting coefficients used to normalize the NMPIW and  $e$ .  $T_{begin}$  and  $T_{end}$  are the start and end temperatures of the simulated annealing algorithm.  $Iter$  is the iterative coefficient, and  $Bolt$  is the Boltzmann constant.

Fig. 8 shows the results obtained when the model parameters were not optimized with the simulated annealing algorithm after the neural network parameters were initialized. Figs. 8(a) and 8(b) show the training result and the prediction performance of the neural network model, respectively. The data show that although the neural network model output could fit the degradation trend, it could not construct an effective prediction interval.

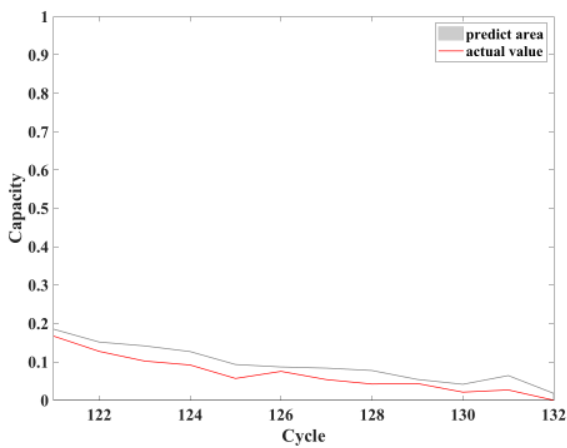




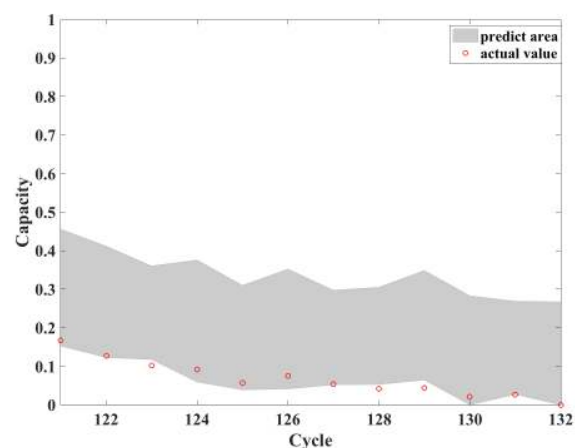
(a) Fitting result of the neural network model



(a) Fitting result of the neural network model



(b) Prediction performance of the neural network model



(b) Prediction performance of the neural network model

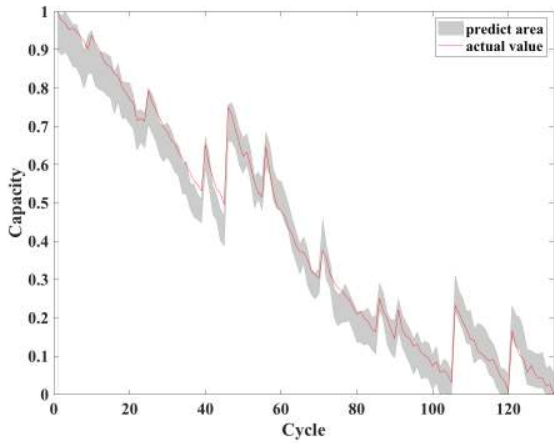
**FIGURE 8.** Fitting result and prediction performance of the neural network model for the #18 battery without optimization by the simulated annealing algorithm.

In Fig. 9, the fitting result and the prediction performance of the neural network model (for the #18 battery) optimized by the simulated annealing algorithm, when  $\mu$  and  $\gamma$  were set to 0.9 and 50, respectively, for initialization, are shown. In the simulated annealing optimization process, the initial average NMPIW was wide, the PICP was small, and the comprehensive indicator CWC was large. During the iteration, the PICP gradually converged to a value slightly higher than the confidence level of 0.9, while the NMPIW gradually narrowed at the beginning to obtain a better prediction interval (high PICP and narrow NMPIW, while the CWC continuously decreased during the process). Finally, a valid prediction interval was obtained from the iteration. The results in Fig. 9(a) show that the LUBE neural network model with the discharge cutoff voltage and SampEn as inputs could simulate the degradation of the battery, while the results in Fig. 9(b) show that the prediction interval could include the actual value. In Fig. 9, because the interval coverage expectation was set too high, the lower bound of the prediction interval reached the failure threshold after the 92<sup>nd</sup> cycle. Meanwhile, the lower bounds

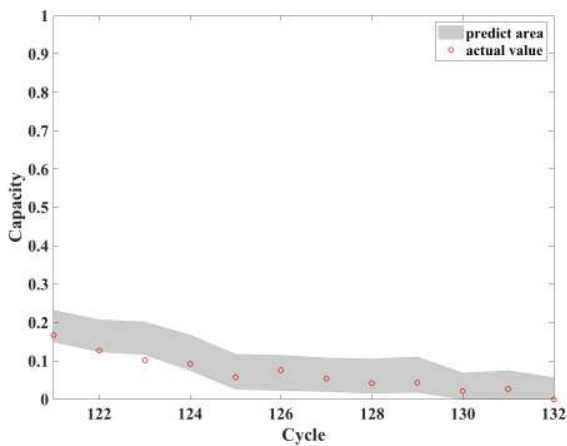
**FIGURE 9.** Fitting result and prediction performance for the #18 battery when  $\gamma$  and  $\mu$  were not optimized.

of the prediction interval from the 110<sup>th</sup> to the 120<sup>th</sup> cycle and from the 123<sup>rd</sup> to the 132<sup>nd</sup> cycle were consistently located at the failure threshold; however, the actual battery SOH failed in the 132<sup>nd</sup> cycle. Although the excessively wide NMPIW ensured the PICP, it also reduced the reliability and practicability of the interval prediction. Therefore, when initializing the LUBE neural network, if  $\mu$  and  $\gamma$  are set too high, overfitting problems will occur.

To increase the PICP while reducing the NMPIW as much as possible, we further conducted a traversal experiment on combinations of  $\mu = \{0.8, 0.82, \dots, 0.96\}$  and  $\gamma = \{10, 15, \dots, 50\}$  and found that when the values of  $\mu$  and  $\gamma$  were set at 0.86 and 40, respectively, the NMPIW could be reduced without greatly affecting the PICP, allowing the minimum integrated indicator CWC to be obtained. At the same time, the modified integrated indicator CWC consists of the PICP, NMPIW, and interval deviation  $e$ , which need to be constrained by  $\beta_1$  and  $\beta_2$  to ensure that the changes remain between 0 and 1. In Fig. 10, the fitting result and prediction performance obtained by adjusting the interval coverage expectation  $\mu$  and the penalty factor  $\gamma$  are shown. As shown



(a) Fitting result of the neural network model



(b) Prediction performance of the neural network model

**FIGURE 10.** Fitting result and prediction performance for the #18 battery after the optimization of  $\mu$  and  $\gamma$ .

in Fig. 10(a), through the above optimization adjustments, a narrow NMPIW was obtained without reducing the PICP. The results in Fig. 10(b) show that the optimized interval prediction lower bound was closer to the actual value; only 1 point fell outside of the interval boundaries, showing excellent prediction performance.

#### IV. COMPARISON EXPERIMENT

To compare the prediction performances of the interval prediction model proposed in this paper and a theoretical interval prediction model, the theoretical interval prediction model using SVM by Widodo [7], with a 90% confidence interval, was selected for experimental comparison. The input  $x$  and output  $y$  can be expressed as follows according to SVM theory [50]:

$$y = f(x) + \zeta \quad (18)$$

where  $\zeta$  is a random variable. We assume that  $\zeta$  and input  $x$  are independent of each other; thus, the calculated confidence interval does not produce a large error in practice.

We define  $\zeta_n$  as

$$\zeta_n = y_n - \hat{f}(x_n) \quad (19)$$

$\zeta$  is usually subject to a zero-mean Gaussian or Laplace distribution, and the Laplace distribution is more suitable in many cases [51]. The Laplace distribution density function with parameter  $\sigma$  is

$$p(z) = \frac{1}{2\sigma} \exp\left(-\frac{|z|}{\sigma}\right) \quad (20)$$

We use  $\zeta_n (n = 1, \dots, N)$  for the sample to estimate  $\sigma$  using the maximum likelihood method, and the maximum likelihood function is

$$L(\sigma; \zeta) = \left(\frac{1}{2\sigma}\right)^N \exp\left(-\frac{|\zeta_1| + \dots + |\zeta_N|}{\sigma}\right) \quad (21)$$

We set  $\frac{\partial \ln L}{\partial \sigma} = 0$ .

$$\hat{\sigma} = \frac{1}{N} \sum_{n=1}^N |\zeta_n| \quad (22)$$

We set  $P(\hat{y} - \Delta \leq y \leq \hat{y} + \Delta) = p_0$ , so

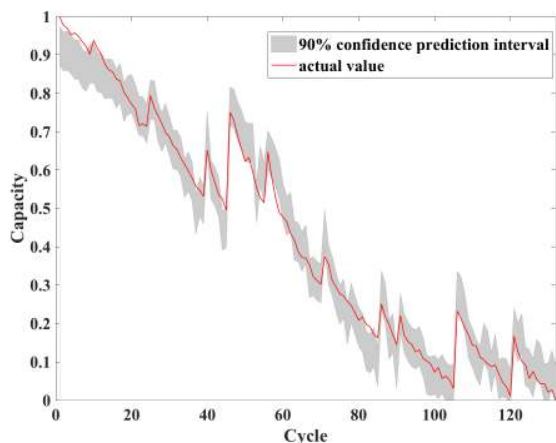
$$p_0 = \int_{-\Delta}^{\Delta} p(\zeta) d\zeta = 1 - \exp\left(-\frac{\Delta}{\hat{\sigma}}\right) \quad (23)$$

$$\Delta = -\hat{\sigma} \ln(1 - p_0) \quad (24)$$

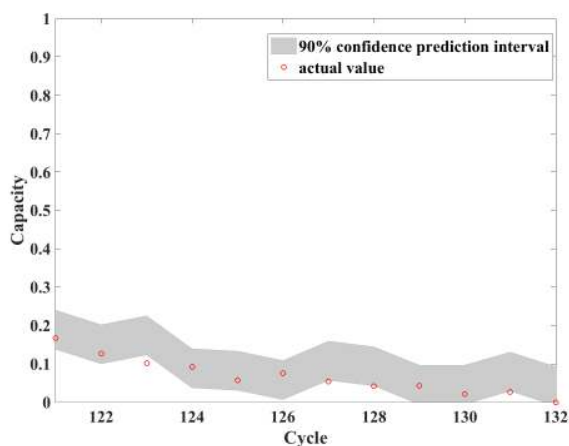
Finally, the confidence interval for the confidence  $p_0$  of the SVM output  $y$  is

$$[\hat{y} + \hat{\sigma} \ln(1 - p_0), \hat{y} - \hat{\sigma} \ln(1 - p_0)] \quad (25)$$

In the experiment, the #18 battery was also selected, the first 120 sets of data were selected as the training set, and the last 12 sets were selected as the test set. For each set of data, the discharge cutoff voltage and SampEn were selected as the inputs and the SOH was used as the output of the SVM method. In terms of parameter settings, the radial basis function (RBF) kernel was also selected to map the inputs, and the RBF kernel parameter  $\gamma$  and the regularization parameter  $C$  were set to 0.4 and 45, respectively. The SVM prediction training results are shown in Fig. 11. The SVM prediction trend was generally consistent with the battery degradation trend; however, three of the prediction results deviated from the 90% confidence interval, mainly because the SVM algorithm is vulnerable to the overfitting problem, causing small fluctuations to be amplified such that they affect the prediction performance. However, the interval prediction method proposed in this paper could include the actual value in the prediction interval, and only one point was outside of the interval boundaries. At the same time, the SVM method estimated the end cycle of the battery SOH as earlier than the actual situation. When the battery SOH estimated by the SVM method reached the failure threshold in the 126<sup>th</sup> cycle, the actual battery SOH still had a 5% remaining capacity. However, the lower bound of the prediction interval obtained with the interval prediction method proposed in this paper reached the failure threshold in the 130<sup>th</sup> cycle and



(a) SVM prediction fitting result



(b) SVM prediction performance

FIGURE 11. SVM prediction performance.

TABLE 2. Prediction performance indicators.

Type of battery	NMPIW	PICP	e	CWC
#18 battery	0.2441	0.7273	3.8670	0.4599
#18 battery after adjustment	0.0858	0.8485	4.0668	0.4232
#18 battery by SVM	0.1016	0.7727	7.2600	0.7565

could provide a reasonable range for the failure threshold of the battery SOH, allowing the ground operator to adjust the battery working state in time.

Finally, the prediction performance of the trained neural network model was measured by four indicators: NMPIW, PICP, e, and CWC. The results are shown in Table 2. The results show that after the model initialization parameters were adjusted, the PICP was higher, the NMPIW was narrower, and the indicating effect of the lower bound of the prediction interval was better.

### V. CONCLUSION

In this study, based on the assessment and prediction requirements of the satellite lithium-ion battery SOH and considering the capacity local recovery effect of satellite lithium-ion

batteries during charge and discharge cycles, a modified LUBE neural network model was constructed in which the discharge cutoff voltage, SampEn based on the discharge voltage, and lithium-ion battery capacity were selected as characteristic parameters. A simulated annealing algorithm was used to optimize the modified comprehensive assessment indicator, CWC. The experimental results based on NASA #18 battery test data show that the proposed method for predicting the lithium-ion battery SOH can successfully predict the degradation trend and local fluctuations of the lithium-ion battery SOH and simultaneously ensure a PICP and an NMPIW that will produce satisfactory performance. When the satellite lithium-ion battery SOH suddenly changes, the comparison of the SOH prediction results with the actual results can provide the ground operators with relevant warnings, showing practicability.

For future work, as the telemetry data sent back by some satellites in orbit to the ground station do not include the battery capacity parameter, and this method cannot directly estimate the degradation of the satellite battery without the capacity data. However, research on the in-orbit satellite lithium-ion battery SOH can be further carried out based on comparisons with a ground battery aging experiment. For example, a same working condition experiment can be conducted by selecting the same battery on the ground, and the ground experimental data can be effectively integrated with the in-orbit telemetry parameters. In addition, the integrated indicator CWC in the LUBE neural network can be further optimized to improve the prediction performance.

### REFERENCES

- [1] K. E. Holbert, G. I. Heydt, and H. Ni, "Use of satellite technologies for power system measurements, command, and control," *Proc. IEEE* vol. 93, no. 5, pp. 947–955, May 2005.
- [2] X. Y. Peng, J. Pang, Y. Peng, and D. Liu, "Review on anomaly detection of spacecraft telemetry data," (in Chinese), *Chin. J. Sci. Instrum.*, vol. 37, no. 9, pp. 1929–1945, 2016.
- [3] B. Zhang, "Evolution and application of PHM technologies," (in Chinese), *Meas. Control Technol.*, vol. 27, no. 2, pp. 5–7, 2008.
- [4] X.-Y. An and L. S. Tan, "Development of lithium-ion batteries as new power sources for space application," *Chin. J. Power Sources*, vol. 30, no. 1, p. 70, 2006.
- [5] N. Miyana, T. Inoue, H. Yoshida, K. Komada, and M. Goto, "Large scale lithium-ion battery cells for space use," in *Proc. 25th Int. Telecommun. Energy Conf.*, Oct. 2003, pp. 241–248.
- [6] D. Liu, J. Zhou, L. Guo, and Y. Peng, "Survey on lithium-ion battery health assessment and cycle life estimation," (in Chinese), *Chin. J. Sci. Instrum.*, vol. 36, no. 1, pp. 1–16, 2015.
- [7] A. Widodo, M.-C. Shim, W. Caesarendra, and B.-S. Yang, "Intelligent prognostics for battery health monitoring based on sample entropy," *Expert Syst. Appl.*, vol. 38, no. 9, pp. 11763–11769, Sep. 2011.
- [8] R. Xiong, J. Cao, Q. Yu, H. He, and F. Sun, "Critical review on the battery state of charge estimation methods for electric vehicles," *IEEE Access*, vol. 6, pp. 1832–1843, 2017.
- [9] W. He, N. Williard, C. Chen, and M. Pecht, "State of charge estimation for electric vehicle batteries using unscented Kalman filtering," *Microelectron. Rel.*, vol. 53, pp. 840–847, Jun. 2013.
- [10] J. Zhang and J. Lee, "A review on prognostics and health monitoring of Li-ion battery," *J. Power Sources*, vol. 196, pp. 6007–6014, Aug. 2011.
- [11] P. A. Topan, M. N. Ramadan, G. Fathoni, A. I. Cahyadi, and O. Wahyunggoro, "State of charge (SOC) and state of health (SOH) estimation on lithium polymer battery via Kalman filter," in *Proc. 2nd Int. Conf. Sci. Technol.-Comput. (ICST)*, Oct. 2016, pp. 93–96.

- [12] M. A. Hannan, M. M. Hoque, A. Hussain, Y. Yusof, and P. J. Ker, "State-of-the-art and energy management system of lithium-ion batteries in electric vehicle applications: Issues and recommendations," *IEEE Access*, vol. 6, pp. 19362–19378, 2018.
- [13] L. Lu, X. Han, J. Li, J. Hua, and M. Ouyang, "A review on the key issues for lithium-ion battery management in electric vehicles," *J. Power Sources*, vol. 226, pp. 272–288, Mar. 2013.
- [14] H. E. Chun and R. Zhang, "Experimentalsummary on IEC 61850internationalinteroperabilitytest," *Autom. Electr. Power Syst.*, vol. 2, pp. 6–10, 2012.
- [15] J. Wu, C. Zhang, and Z. Chen, "An online method for lithium-ion battery remaining useful life estimation using importance sampling and neural networks," *Appl. Energy*, vol. 173, pp. 134–140, Jul. 2016.
- [16] S. S. Y. Ng, Y. Xing, and K. L. Tsui, "A naive Bayes model for robust remaining useful life prediction of lithium-ion battery," *Appl. Energy*, vol. 118, pp. 114–123, Apr. 2014.
- [17] J. X. Zhang, C.-H. Hu, X. He, X.-S. Si, Y. Liu, and D.-H. Zhou, "Lifetime prognostics for deteriorating systems with time-varying random jumps," *Rel. Eng. Syst. Saf.*, vol. 167, pp. 338–350, Nov. 2017.
- [18] Y. Chen, Q. Miao, B. Zheng, S. Wu, and M. Pecht, "Quantitative analysis of lithium-ion battery capacity prediction via adaptive bathtub-shaped function," *Energies*, vol. 6, no. 6, pp. 3082–3096, 2013.
- [19] D. Wang, Q. Miao, and M. Pecht, "Prognostics of lithium-ion batteries based on relevance vectors and a conditional three-parameter capacity degradation model," *J. Power Sources*, vol. 239, pp. 253–264, Oct. 2013.
- [20] M. Kotobuki, Y. Suzuki, H. Munakata, K. Kanamura, Y. Sato, K. Yamamoto, and T. Yoshida, "Effect of sol composition on solid electrode/solid electrolyte interface for all-solid-state lithium ion battery," *Electrochim. Acta*, vol. 56, no. 3, pp. 1023–1029, Jan. 2011.
- [21] S. S. Choi and H. S. Lim, "Factors that affect cycle-life and possible degradation mechanisms of a Li-ion cell based on  $\text{LiCoO}_2$ ," *J. Power Sources*, vol. 111, no. 1, pp. 130–136, Sep. 2002.
- [22] W. Wang, J. Zhu, Y. Zhang, Z. Tian, and X. Wang, "Design for automatic generation of spacecraft telemetry software code based on incremental model," in *Proc. 2nd IEEE Adv. Inf. Manage., Commun., Electron. Automat. Control Conf. (IMCEC)*, May 2018, pp. 1730–1734.
- [23] J. Zhang, X. He, X. Si, C. Hu, and D. Zhou, "A novel multi-phase stochastic model for lithium-ion batteries' degradation with regeneration phenomena," *Energies*, vol. 10, no. 11, p. 1687, Oct. 2017.
- [24] A. Eddahech, O. Briat, and J.-M. Vinassa, "Lithium-ion battery performance improvement based on capacity recovery exploitation," *Electrochim. Acta*, vol. 114, pp. 750–757, Dec. 2013.
- [25] D. Liu, J. Pang, J. Zhou, Y. Peng, and M. Pecht, "Prognostics for state of health estimation of lithium-ion batteries based on combination Gaussian process functional regression," *Microelectron. Rel.*, vol. 53, no. 6, pp. 832–839, 2013.
- [26] Y. J. He, J.-N. Shen, J.-F. Shen, and Z.-F. Ma, "State of health estimation of lithium-ion batteries: A multiscale Gaussian process regression modeling approach," *AICHE J.*, vol. 61, no. 5, pp. 1589–1600, May 2015.
- [27] B. E. Olivares, M. A. Cerda Muñoz, M. E. Orchard, and J. F. Silva, "Particle-filtering-based prognosis framework for energy storage devices with a statistical characterization of state-of-health regeneration phenomena," *IEEE Trans. Instrum. Meas.*, vol. 62, no. 2, pp. 364–376, Feb. 2013.
- [28] L. Tao and C. Lu, "Random forest based Li-Ion battery capacity prediction subject to capacity recovery effect," in *Proc. IEEE Vehicle Power Propuls. Conf. (VPPC)*, Dec. 2017, pp. 1–6.
- [29] J. S. Richman and J. R. Moorman, "Physiological time-series analysis using approximate entropy and sample entropy," *Amer. J. Physiol.-Heart Circulatory Physiol.*, vol. 278, no. 6, pp. H2039–H2049, 2000.
- [30] Y.-H. Sun, H.-L. Jou, and J.-C. Wu, "Aging estimation method for lead-acid battery," *IEEE Trans. Energy Convers.*, vol. 26, no. 1, pp. 264–271, Dec. 2011.
- [31] X. Hu, S. E. Li, Z. Jia, and B. Egardt, "Enhanced sample entropy-based health management of Li-Ion battery for electrified vehicles," *Energy*, vol. 64, pp. 953–960, Jan. 2014.
- [32] X. Hu, J. Jiang, D. Cao, and B. Egardt, "Battery health prognosis for electric vehicles using sample entropy and sparse Bayesian predictive modeling," *IEEE Trans. Ind. Electron.*, vol. 63, no. 4, pp. 2645–2656, Apr. 2015.
- [33] J. Li, L. Wang, C. Lyu, W. Luo, K. Ma, L. Zhang, "A method of remaining capacity estimation for lithium-ion battery," *Adv. Mech. Eng.*, vol. 5, Jan. 2013, Art. no. 154831.
- [34] J. Li, C. Lyu, L. Wang, L. Zhang, and C. Li, "Remaining capacity estimation of Li-Ion batteries based on temperature sample entropy and particle filter," *J. Power Sources*, vol. 268, pp. 895–903, Dec. 2014.
- [35] Z. Wang, S. Zeng, J. Guo, and T. Qin, "State of health estimation of lithium-ion batteries based on the constant voltage charging curve," *Energy*, vol. 167, pp. 661–669, Jan. 2019.
- [36] K. Li, R. Wang, H. Lei, T. Zhang, Y. Liu, and X. Zheng, "Interval prediction of solar power using an Improved Bootstrap method," *Sol. Energy*, vol. 159, pp. 97–112, Jan. 2018.
- [37] Z. Wang, J. Ma, and L. Zhang, "State-of-health estimation for lithium-ion batteries based on the multi-Island genetic algorithm and the Gaussian process regression," *IEEE Access*, vol. 5, pp. 21286–21295, 2017.
- [38] H. Li, D. Pan, and C. L. P. Chen, "Intelligent prognostics for battery health monitoring using the mean entropy and relevance vector machine," *IEEE Trans. Syst., Man, Cybern. Syst.*, vol. 44, no. 7, pp. 851–862, Jul. 2014.
- [39] H. Liu, B. Qi, and M. Zheng, "A new algorithm for the SOH estimation of the single battery in battery-power station," in *Proc. 9th IEEE Conf. Ind. Electron. Appl.*, Jun. 2014, pp. 729–732.
- [40] H. Zhang and S.-S. He, "Analysis and comparison of permutation entropy, approximate entropy and sample entropy," in *Proc. Int. Symp. Comput., Consum. Control (IS3C)*, Dec. 2018, pp. 209–212.
- [41] G. Manis, M. Aktaruzzaman, and R. Sassi, "Low computational cost for sample entropy," *Entropy*, vol. 20, no. 1, p. 61, Jan. 2018.
- [42] R. Alcaraz and J. J. Rieta, "A review on sample entropy applications for the non-invasive analysis of atrial fibrillation electrocardiograms," *Biomed. Signal Process. Control*, vol. 5, no. 1, pp. 1–14, Jan. 2010.
- [43] T. Horie, N. Burioka, T. Amisaki, and E. Shimizu, "Sample entropy in electrocardiogram during atrial fibrillation," *Yonago Acta Medica*, vol. 61, no. 1, pp. 49–57, Mar. 2018.
- [44] W. Sun and Y. Wang, "Short-term wind speed forecasting based on fast ensemble empirical mode decomposition, phase space reconstruction, sample entropy and improved back-propagation neural network," *Energy Convers. Manage.*, vol. 157, pp. 1–12, Feb. 2018.
- [45] H. Wang, C. Wu, T. Li, Y. He, P. Chen, and A. Bezerianos, "Driving fatigue classification based on fusion entropy analysis combining EOG and EEG," *IEEE Access*, vol. 7, pp. 61975–61986, 2019.
- [46] A. Khosravi, S. Nahavandi, D. Creighton, and A. F. Atiya, "Comprehensive review of neural network-based prediction intervals and new advances," *IEEE Trans. Neural Netw.*, vol. 22, no. 9, pp. 1341–1356, Sep. 2011.
- [47] L. G. Marín, F. Valencia, and D. Sáez, "Prediction interval based on type-2 fuzzy systems for wind power generation and loads in microgrid control design," in *Proc. IEEE Int. Conf. Fuzzy Syst. (FUZZ-IEEE)*, Jul. 2016, pp. 328–335.
- [48] D. Zhao, P. Guo, and P. Zhao, "Estimating model of standard enthalpy of intermetallics," *J. Central South Univ. (Sci. Technol.)*, vol. 42, no. 6, pp. 1578–1583, Jun. 2011.
- [49] G. H. R. Kegel, R. J. Laramée, and B. D. Bhardwaj, "The free energy of mixing in the lithium-germanium binary system," *J. Electrochem. Soc.*, vol. 118, no. 10, pp. 1662–1665, 1971.
- [50] J. Wang et al., "Remaining useful life interval estimation for machine parts based on SVM," *J. Northeastern Univ.*, 2016.
- [51] B. Jiang, X. Zhang, and T. Cai, "Estimating the confidence interval for prediction errors of support vector machine classifiers," *J. Mach. Learn. Res.*, vol. 9, pp. 521–540, Mar. 2008.



**MENGDA CAO** received the B.E. degree from the College of Environmental and Resource Science, Zhejiang University (ZJU), Hangzhou, China, in 2017. He is currently pursuing the master's degree with the National University of Defense Technology (NUDT).



**TAO ZHANG** received B.S., M.S., and Ph.D. degrees from the National University of Defense Technology (NUDT), Changsha, China, in 1998, 2001, and 2004, respectively.

He is currently a Professor with the College of Information System and Management, NUDT. His current research interests include multicriteria decision making, optimal scheduling, data mining, and optimization methods on energy Internet networks.



**YAJIE LIU** was born in 1975. He is currently pursuing the Ph.D. degree with the College of System Engineering, National University of Defense Technology, China, where he is also an Associate Professor.

He was a Visiting Scholar with the Mechanical and Industrial Engineering Department, University of Toronto, from 2008 to 2009. His current research interests include planning, optimization methods of microgrids, and data-driven PHM.

...



**BIN YU** received the B.E. degree from the School of Aeronautics, Northwestern Polytechnical University, Xi an, China, and the M.S. degree from the College of Systems Engineering, National University of Defense Technology (NUDT), Changsha, China.

He is currently the Director of Materials Management Office, China Aerospace Science and Technology Corporation. His current research interests include aerospace engineering management and supply chain management.